Electronic Structure of Disordered CuPd Alloys: A Two-Dimensional Positron-Annihilation Study

L. C. Smedskjaer, R. Benedek, R. W. Siegel, D. G. Legnini, and M. D. Stahulak
Materials Science Division, Argonne National Laboratory, Argonne, Illinois 60439

and

A. Bansil
Physics Department, Northeastern University, Boston, Massachusetts 02115
(Received 30 April 1987)

Two-dimensional–angular-correlation experiments using positron-annihilation spectroscopy were performed on a series of disordered Cu-rich CuPd-alloy single crystals. The results are compared with theoretical calculations based on the Korringa-Kohn-Rostoker coherent-potential approximation. Our experiments confirm the theoretically predicted flattening of the alloy Fermi surface near [110] with increasing Pd concentration. The momentum densities and the two-dimensional–angular-correlation spectra around zero momentum exhibit a characteristic signature of the electronic states near the valence-band edge in the alloy.

PACS numbers: 71.25.Hc, 78.70.Bj

Two-dimensional angular correlation (2D-ACAR) using positron-annihilation spectroscopy (PAS) is a powerful tool for studying the electronic structure in concentrated alloys. The unique capabilities of the method were demonstrated in an early experiment on CuZn alloys by Haghgooie and Berko.[1] The full potential of 2D-ACAR, however, can only be realized when measurements are complemented by corresponding electronic-structure calculations. Recently, the Korringa-Kohn-Rostoker (KKR) coherent-potential-approximation (CPA) method has been adapted to the calculation of momentum densities in disordered alloys.[2-4] With this development, as well as improvements in 2D-ACAR detection systems,[5] it is timely to make a renewed investigation of disordered alloys with the 2D-ACAR technique.

This Letter reports experimental and theoretical results for the α-phase CuPd system, which has recently attracted considerable attention.[6,7] In these alloys, the overlap between the Cu and Pd d bands leads to a strong hybridization that gives rise to an electronic structure which is in marked contrast to that found in the pure materials. KKR CPA calculations predict an appreciable flattening of the Fermi surface (FS) along the [110] direction up to about 40 at.% Pd. This flattening is thought to be responsible for the short-range order that has been observed by diffuse electron[8] and x-ray[9] scattering.

The present work focuses on two aspects of the CuPd system, namely the FS dimensions in the [100] and [110] directions as a function of Pd concentration and the behavior of the momentum density $\rho(\mathbf{p})$ near zero momentum. Our results provide the first direct experimental evidence that the FS of Cu does indeed flatten in the vicinity of [110] upon the addition of Pd. 2D-ACAR PAS measurements on these systems also yield significant information near the central peak at zero momentum. The momentum density $\rho(\mathbf{p})$ near $\mathbf{p}=0$ reflects changes in the nature of electronic states near the valence-band edge and is sensitive to alloying. PAS therefore provides a probe of such low-lying states, which are inaccessible to other experimental techniques. This aspect of the 2D-ACAR spectra has not been explored previously.

Measurements were performed on $Cu_{1-x}Pd_x$ ($x=0$, 0.10, 0.15, 0.20, and 0.25) single-crystal specimens, with [100] directions aligned normal to the faces of the Anger cameras.[10] 2D-ACAR spectra based on $(1.5-2.0)\times10^7$ counts and a channel width of 0.17 mrad were obtained for the $x=0.0$, 0.15, and 0.25 specimens. In addition, spectra with 2×10^6 counts and 0.34-mrad channel width were taken for all of the specimens. All spectra were corrected for the momentum-dependent efficiency of the cameras. The instrumental resolution was 0.34×0.34 mrad^2, but since all measurements were made at room temperature this must be corrected for the thermal motion of the positron, yielding an effective resolution of 0.6×0.6 mrad^2.

Calculations based on the KKR CPA method were performed for CuPd alloys with $x=0.15$ and 0.25 as well as pure Cu. The muffin-tin potentials used here are identical to those used in earlier work.[7] The formulation of the momentum density within the KKR CPA is described in Refs. 2 and 3; in the case of pure Cu, calculations were performed with the KKR method.[11] For Cu, both the electron momentum density $\rho(\mathbf{p})$ and the two-photon momentum density $\rho_{2\gamma}(\mathbf{p})$ were calculated, but for the alloys only $\rho(\mathbf{p})$ was obtained. [Note that our calculations in alloys thus correspond to the use of a constant positron wave function in a $\rho_{2\gamma}(\mathbf{p})$ computation.] The difference between the calculated $\rho_{2\gamma}(\mathbf{p})$ and $\rho(\mathbf{p})$ is relatively small at low momenta (p less than the Fermi momentum) and their qualitative features are similar.

The momentum density was calculated on a grid of points in the (001) and (011) planes in reciprocal space. Sections of 2D-ACAR spectra along the [100] and [110] directions were then constructed by integration of the momentum density.

The FS radii in various directions are in principle given by the positions of extrema in the derivative of the 2D-ACAR spectra. The finite instrumental resolution, however, can shift the positions of the extrema and in general a more detailed analysis is required. In this connection, we have carried out a number of studies including simulations using theoretical $\rho(\mathbf{p})$ curves convoluted with the experimental resolution function and the use of a high-pass filter on the differentiated data. Our conclusion is that for Cu and the CuPd alloys considered here, the Fermi radius along [110] may be determined via a simple differentiation of the 2D-ACAR spectra, but a more detailed procedure is required for extracting the [100] FS radius.

The [100] FS radius k_F was determined by fitting the data in the vicinity of k_F with a model 2D-ACAR spectrum $N(p_x,p_y)$ parametrized in terms of elliptical and Gaussian terms[12]:

$$N(p_x,p_y)=I_1E(p_x,p_y)+I_2G(p_x,p_y), \tag{1}$$

where

$$E(p_x,p_y)=\begin{cases}[1-(p_x/k_F)^2]-(p_y/k_t)^2]^{1/2}, & \text{for } (p_x/k_F)^2+(p_y/k_t)^2<1,\\ 0, & \text{for } (p_x/k_F)^2+(p_y/k_t)^2\geqq 1,\end{cases} \tag{2}$$

$$G(p_x,p_y)=\exp\{-\tfrac{1}{2}[(p_x/\sigma_F)^2+(p_y/\sigma_t)^2]\}. \tag{3}$$

After convolution of Eq. (1) with the instrumental resolution function, least-squares fits of the parameters I_1, I_2, σ_F, σ_t, k_t, and k_F were made directly to the as-observed data (no symmetry was enforced) in four local regions around k_F with a diameter of 3.5 mrad each.

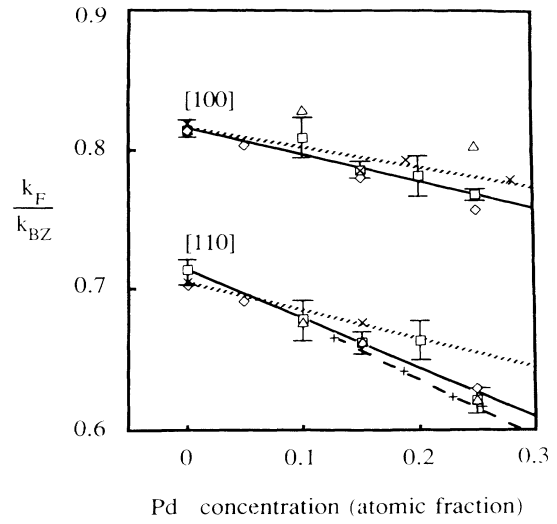

FIG. 1. k_F/k_{BZ}, where k_F is the FS radius in a given direction and k_{BZ} is the Brillouin-zone dimension along the same direction, as a function of Pd concentration. Results for the [100] and [110] directions are shown. Solid lines are the least-squares fits to the FS radii deduced from the present experiments, (squares); the slopes of the lines are determined to be -0.19 ± 0.03 and -0.34 ± 0.05, respectively, for the [100] and [110] directions. Theoretical results are as follows: lozenges, present work and Rao *et al.* (Ref. 7); triangles, Gyorffy and Stocks (Ref. 6). Least-squares linear fits to the data of Hasegawa, Suzuki, and Hirabayashi (crosses and dotted lines, Ref. 14) and Oshima and Watanabe (plusses and dashed line, only for [110], Ref. 8) are also shown.

Since $\sigma_F\neq\sigma_t$ and $k_F\neq k_t$, this model allows for asphericity of FS in the vicinity of [100]. The values of k_F deduced in this manner were insensitive both to the size of the local region and to the assumed instrumental resolution function.

Our results for the [100] and [110] FS radii[13] are compared in Fig. 1 with calculations of Rao *et al.*[7] (which are extended here to $x=0.25$) and Gyorffy and Stocks.[6] The agreement between theory and experiment is excellent, particularly with respect to the concentration dependence of the radii. The more rapid decrease of k_F/k_{BZ} with Pd concentration in the [110] direction compared with that in the [100] direction indicates a flattening of the FS in the vicinity of [110] upon addition of Pd. We note that although the two sets of theoretical predictions for the [100] direction differ in absolute mag-

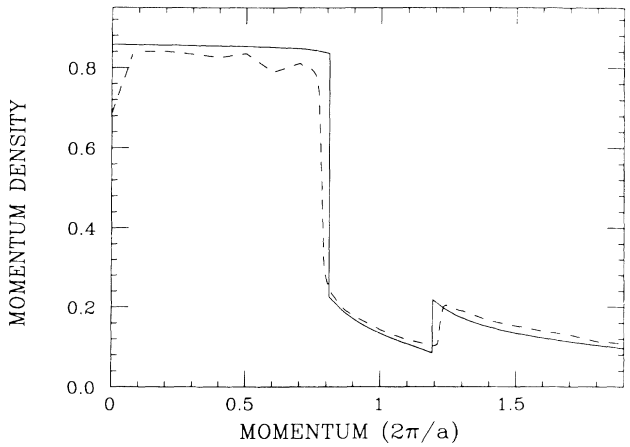

FIG. 2. Momentum density $\rho(\mathbf{p})$ in Cu (solid line) and $Cu_{85}Pd_{15}$ (dashed line) along the [100] direction in the Brillouin zone.

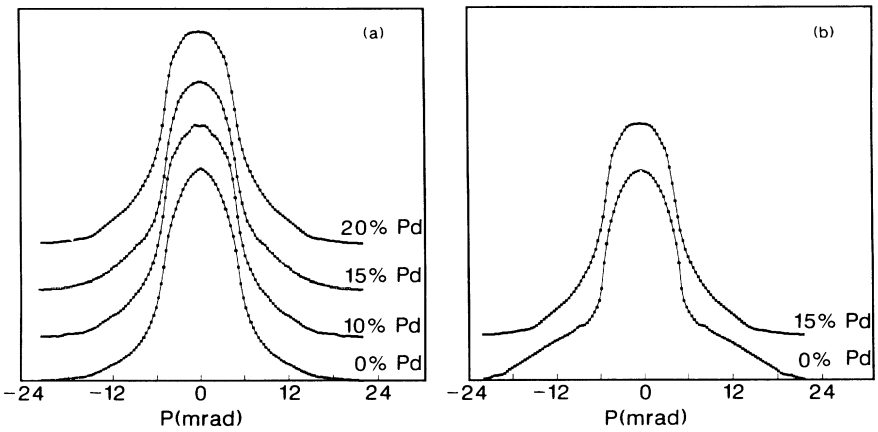

FIG. 3. (a) Experimental and (b) theoretical [100] sections of the [001] 2D-ACAR surface for CuPd alloys. The theoretical curves are computed with a constant positron wave function (see text).

nitude, both yield essentially the same slope and hence a similar flattening effect. Figure 1 shows that the present experimental results differ substantially from the previous crossed-slit measurements on CuPd alloys by Hasegawa, Suzuki, and Hirabayashi.[14] The slope of our k_{110} line is seen to be in good accord with the valued deduced by Oshima and Watanabe[8] from diffuse electron scattering.

We have also investigated the composition dependence of the FS of Cu within the rigid-band model[15] and by application of the KKR CPA for several transition and nontransition solutes. It is a general characteristic of these calculations that the FS of Cu alloys flattens in the vicinity of [110] with decreasing electron/atom ratio. These results, together with the present measurements, leave little doubt that the flattening indeed occurs.

We note that the FS of Cu remains quite sharp on alloying with Pd. As demonstrated in Fig. 2, which compares $\rho(\mathbf{p})$ along [100] in Cu and $Cu_{85}Pd_{15}$, the FS breaks in Cu around 0.8 and 1.2 units continue to be well defined in $Cu_{85}Pd_{15}$. In certain other alloys, such as CuGe, these FS breaks are considerably smeared out as a result of disorder scattering.[16]

We address now the behavior of $\rho(\mathbf{p})$ near $\mathbf{p}=0$. Figure 2 shows that $\rho(\mathbf{p})$ in the 15-at.% Pd alloy possesses a local minimum around $\mathbf{p}=0$. Because of the momentum and angular momentum selection rules only states near the valence-band edge contribute to $\rho(\mathbf{p})$ near $\mathbf{p}=0$. Furthermore, the momentum density reflects the spatial character of the wave functions of these states: $\rho(\mathbf{p}=0)$ is large when the wave functions are relatively smooth [as in a free-electron gas, where $\rho(0)=1$, the maximum allowed value]; fluctuations in the wave function, on the other hand, tend to reduce the value of $\rho(0)$. The decrease in $\rho(0)$ in $Cu_{85}Pd_{15}$ in Fig. 2 indicates that the electronic states associated with the valence-band edge (Γ_1) in the alloy exhibit substantially more fluctuations (and thus possess a larger fraction of high-momentum components) than those in pure Cu.

Figure 3 shows sections of the experimental and theoretical 2D-ACAR surfaces for pure Cu and several CuPd alloys. It is evident that the addition of Pd causes a distinct flattening of these 2D-ACAR sections near $\mathbf{p}=0$ both in the theoretical predictions and in the experimental observations. We find that a substantial part of this flattening is associated with the dip in $\rho(\mathbf{p})$ in the alloy at $\mathbf{p}=0$ (cf. Fig. 2). Since 2D-ACAR is an integrated property [requiring a one-dimensional integration of $\rho(\mathbf{p})$ over one of the momentum variables], a given feature cannot of course be attributed entirely to the behavior of $\rho(\mathbf{p})$ in a single region of momentum space. A variety of other changes in the 2D-ACAR spectra [e.g., changes in the region between 5 and 18 mrad in Fig. 3(a)] on alloying will be discussed elsewhere.

We are grateful to Dr. P. E. Mijnarends for illuminating discussions and for making available his 2D-ACAR results on CuGe single crystals prior to publication. This work was supported by the U.S. Department of Energy, Basic Energy Science-Materials Sciences, under Contracts No. W-31-109-Eng-38 and No. DE-FG02-85ER45223, and benefitted from an allocation of time on the ER-Cray computer at Lawrence Livermore National Laboratory.

[1]M. Haghgooie and S. Berko, in *Positron Annihilation,* edited by R. R. Hasiguti and K. Fujiwara (Japan Institute of Metals, Sendai, Japan, 1979), p. 291. See also the review by S. Berko, *ibid.* and references therein.

[2]A. Bansil, R. S. Rao, P. E. Mijnarends, and L. Schwartz, Phys. Rev. B **23**, 3608 (1981).

[3]A. Bansil and P. E. Mijnarends, Phys. Rev. B **30**, 628 (1984).

[4]Z. Szotek, B. L. Gyorffy, G. M. Stocks, and W. M. Temmerman, J. Phys. F **14**, 2571 (1984).

[5]See, e.g., L. C. Smedskjaer and M. J. Fluss, in *Methods of*

Experimental Physics (Academic, New York, 1983), Vol. 21, p. 77.

[6]B. L. Gyorffy and G. M. Stocks, Phys. Rev. Lett. **50**, 374 (1983).

[7]R. S. Rao, A. Bansil, H. Asonen, and M. Pessa, Phys. Rev. B **29**, 1713 (1984).

[8]K. Oshima and D. Watanabe, Acta Crystallogr., Sect. A **29**, 520 (1973).

[9]K. Oshima, D. Watanabe, and J. Harada, Acta Crystallogr., Sect. A **32**, 883 (1976).

[10]The Anger cameras, manufactured by General Electric, each consisted of a NaI(Tl) crystal with an overall diameter of about 620 mm backed by 91 phototubes. The geometrical resolution on the surface of each camera was 2.7–3-mm FWHM at 511 keV and the distance from the source to each of the cameras was about 12.5 m. Each camera provided, by means of a hybrid computer, output signals corrected for imaging errors and energy deficiencies.

[11]P. E. Mijnarends, in *Positron Solid State Physics,* International School of Physics "Enrico Fermi," Course 83, edited by W. Brandt (North-Holland, Amsterdam, 1983).

[12]In the present experimental geometry, the projections of the FS in the first and second zones overlap along [110]. (In addition the necks project onto this direction.) Therefore, it is not sensible to model k_{110} in the manner of k_{100} with Eqs. (1)–(3). A better approach will be to measure a more favorable crystal orientation. While error bars on k_{110} could be reduced substantially by a more sophisticated analysis of the data and/or additional measurements, our determination of k_{110} from peak positions in the differentiated spectra is considered adequate for the present purposes.

[13]The experimental values for pure Cu in Fig. 1 are in good accord with the values obtained from de Haas–van Alphen measurements.

[14]M. Hasegawa, T. Suzuki, and M. Hirabayashi, J. Phys. Soc. Jpn. **43**, 89 (1977).

[15]A rigid-band computation using our Cu potential yields k_{100} and k_{110} values very close to the KKR CPA points of Rao *et al.* in Fig. 1.

[16]R. Prasad and A. Bansil, Phys. Rev. Lett. **48**, 113 (1982).